Journal of Chromatography A, 1218 (2011) 1530–1537

Contents lists available at ScienceDirect

Journal of Chromatography A

journal homepage: www.elsevier.com/locate/chroma

Adsorption of deamidated antibody variants on macroporous and dextran-grafted cation exchangers: II. Adsorption kinetics

Yinying Tao [a], Giorgio Carta [a,*], Gisela Ferreira [b], David Robbins [b]

[a] Department of Chemical Engineering, University of Virginia, 102 Engineers' Way, Charlottesville, VA 22904-4741, USA
[b] MedImmune, One MedImmune Way, Gaithersburg, MD 20877, USA

ARTICLE INFO

Article history:
Received 29 October 2010
Received in revised form 13 January 2011
Accepted 17 January 2011
Available online 22 January 2011

Keywords:
Monoclonal antibody charge variants
Ion exchange
Multicomponent adsorption kinetics
Mass transfer modeling

ABSTRACT

Single and multicomponent batch adsorption kinetics were obtained for deamidated mAb variants on two commercial cation exchangers, one with an open macroporous structure – UNOsphere S – and the other with charged dextran grafts – Capto S. The adsorption kinetics for the macroporous matrix was found to be controlled largely by pore diffusion. The effective diffusivity estimated from single component data was a fraction of the mAb free solution diffusivity, and its value could be used to accurately predict the adsorption kinetics for two- and three-component systems. In this case, when two or more variants were adsorbed simultaneously, both experimental and predicted results showed a temporary overshoot of the amount adsorbed above the equilibrium value for the more deamidated variant followed by a gradual approach to equilibrium. Adsorption rates on the dextran grafted material were much faster than those observed for the macroporous matrix for both single component and simultaneous adsorption cases. In this case, no significant overshoot was observed for the more deamidated forms. The Capto S adsorption kinetics could be described well by a diffusion model with an adsorbed phase driving force for single component adsorption and for the simultaneous adsorption of multiple variants. However, this model failed to predict the adsorption kinetics when more deamidated forms pre-adsorbed on the resin were displaced by less deamidated ones. In this case, the kinetics of the displacement process was much slower indicating that the pre-adsorbed components severely hindered transport of the more strongly bound variants. Overall, the results indicate that despite the lower capacity, the macroporous resin may be more efficient in process applications where displacement of one variant by another takes place as a result of the faster and more predictable kinetics.

1. Introduction

In Part I of this work [1], we investigated the cation exchange adsorption equilibrium properties of deamidated forms of a monoclonal antibody (mAb). Deamidation of mAbs is often a serious concern since it can occur in parts of the molecule that may affect the bioactivity thereby reducing or even compromising the therapeutic efficiency of this important class of biopharmaceuticals [2,3]. The separation of deamidated forms may therefore be desirable for the manufacturing of therapeutic proteins [4,5]. Ion exchange chromatography has been successfully applied for this purpose at the analytical scale as deamidation produces charge differences from the conversion of asparagine and glutamine residues into aspartic and glutamic acid residues, respectively [6–9]. In our prior work, we characterized the single and multicomponent adsorption equilibrium of deamidated variants on the cation exchangers UNOsphere S from Bio-Rad Laboratories (Hercules, CA, USA) and Capto S from GE Healthcare (Piscataway, NJ, USA). The former possesses a macroporous architecture while the latter is based on a crosslinked agarose matrix functionalized with charged dextran grafts. No selectivity was seen at pH 5 for either stationary phase. Although the binding strength was lower, both matrices exhibited substantial selectivity at pH 7.5. The effective binding charge of the antibody, determined from linear gradient elution experiments and from the steric mass action (SMA) model, differed between the two different matrices, but was nearly independent of the degree of deamidation. For both materials predictions of multicomponent adsorption based on SMA parameters determined from single component measurements were in good agreement with experimental results indicating that the different variants bind in competition with each other.

Besides adsorption equilibrium, the adsorption kinetics is also important in the design of protein chromatography processes at the industrial scale where diffusional mass transfer within the particles is typically rate limiting [10,11]. Thus, understanding the rates and mechanism of intraparticle transport is critical [12,13]. Protein

* Corresponding author. Tel.: +1 434 924 6281; fax: +1 434 982 2658.
E-mail address: gc@virginia.edu (G. Carta).

0021-9673/$ – see front matter © 2011 Elsevier B.V. All rights reserved.
doi:10.1016/j.chroma.2011.01.050

adsorption kinetics in ion exchangers have been studied extensively for single component systems using a variety of macroscopic and microscopic techniques [12–20] and it has been found that different diffusion mechanisms can be controlling depending on pH, salt concentration and the characteristics of protein and stationary phases [21–23]. In general, pore diffusion is dominant for macroporous matrices, when the pore size is much larger than the size of the protein molecules. In this case, the mass transfer flux is proportional to the gradient in protein concentration in the particle pores [11,12]. A different mass transfer mechanism apparently driven by a gradient in adsorbed protein concentration has, however, been observed for certain conditions where protein transport occurs in close proximity to the adsorbent surface or within flexible charged polymer gels [14,24–28]. For such conditions, since the adsorbed protein concentration gradient can give a large driving force, mass transfer can be faster despite the reduced molecular mobility of the protein in the adsorbed state [13,14,29].

Despite the substantial differences, for practical calculations the mass transfer flux can be described for both mechanisms discussed above using a phenomenological effective pore diffusivity, D_e. When macropore diffusion is controlling, D_e is usually relatively independent of protein and salt concentration, and is related to the free solution diffusivity, D_0, by the following equation [11,29]:

$$D_e = \frac{\psi_p \varepsilon_{pM} D_0}{\tau_p} \quad (1)$$

where ε_{pM} is the particle macroporosity, τ_p the tortuosity factor, and ψ_p the diffusional hindrance factor [30]. The latter varies somewhat with salt concentration as a result of electrostatic effects [31] or when the bound protein restricts the pore size. However, these effects are usually small for large pore matrices. On the other hand, when diffusion is driven by the gradient in adsorbed phase concentration, the apparent D_e dependency on protein and salt concentration may be described by the following approximate relationship [14,32,33]:

$$D_e \sim D_s \frac{q^*}{C} \quad (2)$$

where D_s is the diffusivity in the adsorbed phase and q^* and C are the adsorbed and solution protein concentrations, respectively. In this case, if D_s is constant and the isotherm is nearly rectangular (i.e. q^* is independent of C), D_e becomes inversely proportional to C.

The description of multicomponent protein adsorption kinetics is relatively straightforward when pore diffusion is dominant provided the kinetics of displacement of a bound protein by another is fast. In this case, the effective pore diffusivity can be expected to be the same as that for each single component system. For these conditions, the effect of competitive binding is a continuous displacement process within the adsorbent particles where the more weakly bound species diffuse toward the center of the particle ahead of the more strongly bound components temporarily reaching average adsorbed concentrations that exceed the equilibrium value. Over time, the more strongly adsorbed components displace the more weakly bound ones eventually reaching the particle center when equilibrium is established. Such a mechanism has been observed experimentally for mixtures of cytochrome c and myoglobin in controlled pore glass [34], and for mixtures of cytochrome c and lysozyme in SP-Sepharose-FF [35] and is consistent with confocal microscopy observations for albumin-IgG mixtures [36] and with theoretical calculations in refs. [34,35,37].

On the other hand, when transport occurs with an adsorbed phase concentration driving force, multicomponent adsorption can be much more difficult to predict since the adsorbed phase diffusivities are not necessarily constant and a simple relationship between D_e and D_s may not exist. For example, Lewus and Carta [38] showed that the simultaneous adsorption kinetics of cytochrome c/lysozyme mixtures on S-HyperD-M (BioSepra, Marlborough, MA, USA) could not be described with constant diffusivities but could be predicted with some accuracy assuming that the driving force is proportional to the chemical potential gradient. Russell and Carta [39] observed microscopically smooth patterns consistent with a co-diffusion process during the co-adsorption of ovalbumin and BSA in cationic polyacrylamide gels. Unfortunately, however, scant details are available in the literature regarding multicomponent protein adsorption kinetics for more realistic systems. As a result, generalizing these observations is uncertain. Thus, in this work we have studied the single and multi component adsorption kinetics of deamidated mAb variants for both UNOsphere S and Capto S matrices and for both simultaneous and sequential adsorption. In the former case, two or more proteins are adsorbed simultaneously on a clean adsorbent, while in the latter a pre-adsorbed protein is displaced by a more strongly adsorbed one. Pore and surface diffusion models are applied to determine the respective pore and solid diffusivities and to make predictions of multicomponent adsorption kinetics for both cases.

2. Experimental

2.1. Materials

The two cation exchangers used in this work are the same as those considered in Part I [1]. UNOsphere S (Bio-Rad Laboratories, Hercules, CA, USA) is a polymeric resin having an open macroporous structure with an apparent pore radius around 68 nm based on the size exclusion characteristics of neutral dextran probes. Capto S (GE Healthcare, Piscataway, NJ, USA) is based on dextran-grafted agarose and has a much smaller apparent pore size that varies from about 5 nm at low ionic strength to about 9 nm in 1 M NaCl. Since, based on the Stokes–Einstein equation, the mAb hydrodynamic radius is around 5 nm, it is clear that diffusional transport in this material is likely to be strongly influenced by interactions with the charged polymer grafts.

As described in Part I [1], three different fractions of a deamidated mAb mixture were separated by cation exchange chromatography using a Source 30S column from GE Healthcare (Piscataway, NJ, USA). These three fractions, identified simply as fractions 1, 2 and 3, were shown to have different degrees of deamidation and binding strengths, with fraction 1 being the most deamidated and most weakly binding one and fraction 3 being the least deamidated and most strongly binding one. Although each fraction contained a mixture of subspecies resolved by high resolution HPLC and by isoelectric focusing (IEF), we assumed that each could be treated as a pseudo-component since no resolution of the subspecies could be seen with the preparative ion exchangers used in this work. Forrer et al. [40] successfully used a similar approach lumping multiple closely related species together into pseudo-components in their description of polyclonal IgG adsorption. Individual fractions and their mixtures reconstituted in different proportions with respect to the original mixture were thus used to study single and multicomponent adsorption kinetics. All other chemicals and reagents were purchased from Fisher Scientific (Pittsburgh, PA, USA) unless otherwise stated.

2.2. Methods

2.2.1. Chromatographic analysis for non-binding conditions

Measurements of the height equivalent to a theoretical plate (HETP) were used initially to determine the protein mass transfer properties of both stationary phases using non-binding conditions to avoid the potential influences of factors related to binding kinet-

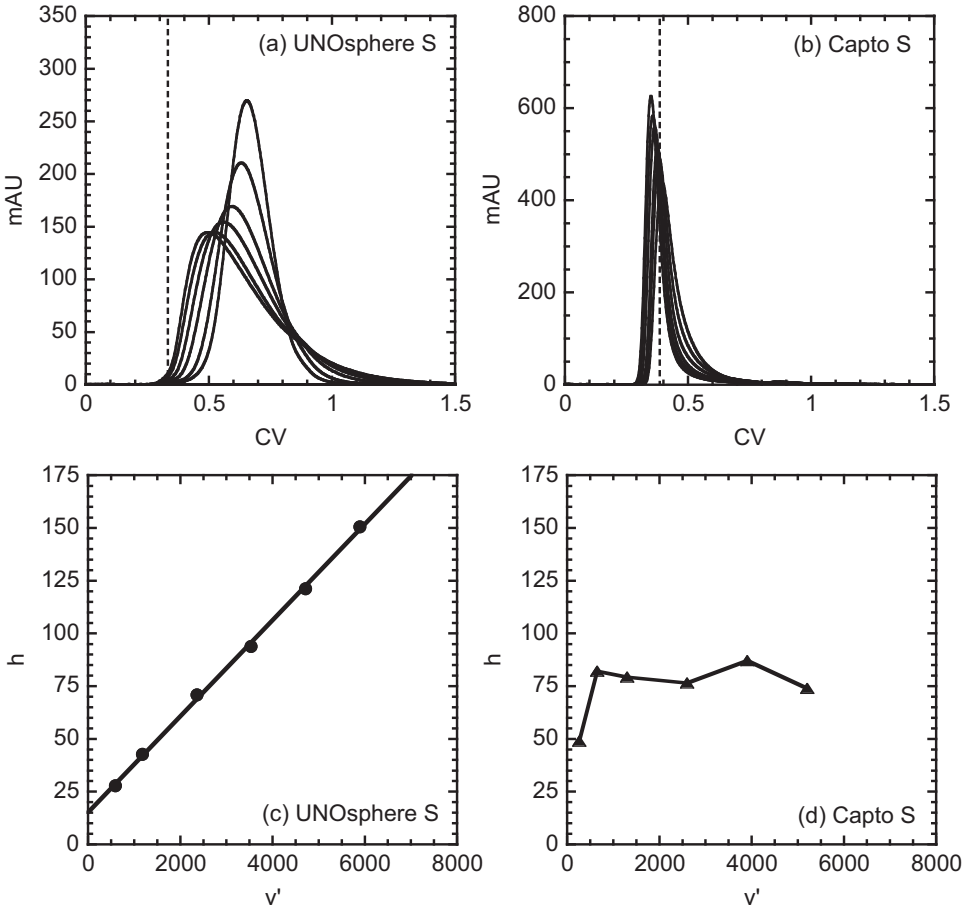

Fig. 1. Overlaid isocratic pulse response peaks under nonbinding conditions for mAb fraction 3 in 1 M NaCl and dimensionless van Deemter curves for UNOsphere S (a and c) and Capto S (b and d). Mobile phase superficial velocities for the curves shown were 0.64, 1.4, 2.6, 3.8, 5.1, and 6.4 cm/min for UNOsphere S, and 0.25, 0.64, 1.4, 2.6, 3.8, 5.1 cm/min for Capto S, respectively. Vertical dashed lines in a and b indicate CV = ε.

ics. The experiments were conducted in 10 mM Na_2HPO_4 buffer at pH 7.5 containing 1 M NaCl, using slurry-packed 1 cm × 10 cm Tricorn columns from GE Healthcare. Since there was no binding under these conditions, the behavior of the different mAb fractions was the same. The HETP was obtained using the moment method [11] and the effective pore diffusivity, D_e, was calculated from the slope of plots of reduced HETP, h (= HETP/d_p) vs. reduced velocity, ν' (= $\nu d_p/D_0$) using the following equation [12]:

$$\frac{D_e}{D_0} = \frac{1}{30}\frac{\varepsilon}{1-\varepsilon}\left(\frac{k'}{1+k'}\right)^2 \frac{d\nu'}{dh} \quad (3)$$

where d_p is the particle diameter, ν the mobile phase interstitial velocity, ε the extraparticle porosity, D_0 the protein free solution diffusivity, and k' the retention factor.

2.2.2. Adsorption kinetics

Batch uptake experiments were performed as described in refs. [12,28]. For one-component measurements, a known amount of adsorbent particles was added to a glass vessel containing 20 ml of protein solution agitated with a paddle-type immersion mixer at 300 rpm. The 280 nm absorbance of the solution recirculated through a UV detector was used to obtain the residual protein concentration and the amount of protein bound was estimated by material balance calculation. Multi-component measurements were done similarly but with a 100 ml of protein solution and withdrawing 300 μl samples at periodic time intervals. These samples were analyzed chromatographically as described in Part I of this work using a 5 mm × 50 mm Source 30S column at 1 ml/min with a 30-column volume (CV) linear gradient from 25 to 60 mM NaCl in 10 mM Na_2HPO_4 at pH 7.5. For both single and multicomponent cases, the amount of clean resin added for each run was in an amount intended to make the final protein concentration in solution equal to about 50% of the initial value based on the equilibrium adsorption capacity as predicted in [1]. Sequential adsorption studies were conducted by first exposing the adsorbent samples to the more weakly bound mAb fraction and then adding a bolus of the more strongly bound fraction, after which the solution concentrations of both species were monitored over time.

3. Results

3.1. Mass transfer kinetics for non-binding conditions

Fig. 1 shows the elution chromatograms and the corresponding plots of h vs. ν' for both UNOsphere S and Capto S at different superficial velocities. Since there was no binding retention occurred only because of diffusion in the particle pores. As seen in this figure, the two matrices gave very different results. For UNOsphere S, the peaks eluted at CV-values significantly larger than the extraparticle porosity ε, and they became broader and more skewed as the flow rate was increased indicating that the protein diffused into the particle pores. On the other hand, for Capto S the peaks were narrow but highly asymmetrical and eluted at CV-values that nearly coincided with the extraparticle porosity, indicating that the mAb molecules were essentially completely excluded from the pores of this matrix under these nonbinding conditions. These results are

consistent with the iSEC experiments obtained with neutral dextran probes described in Part I of this work [1] that gave an apparent pore radius of about 5 nm for Capto S, nearly the same as the mAb hydrodynamic radius. Accordingly, the HETP vs. flow velocity plots in Fig. 1c and d show a linear relationship for UNOsphere S but a flat line for Capto S. Based on Eq. (3), the UNOsphere S results gave $D_e/D_0 = 0.18 \pm 0.02$ or $D_e = 6.8 \pm 0.3 \times 10^{-8}$ cm^2/s, based on the estimated free solution diffusivity $D_0 = 3.8 \times 10^{-7}$ cm^2/s. Since for UNOsphere S the macroporosity is $\varepsilon_{pM} = 0.58$ [1] and ψ_p is estimated to be around 1 because of the large ratio of pore and protein sizes [30], Eq. (1) gives $\tau_p \sim 3$, which is in the range normally encountered for ordinary diffusion in macroporous matrices [41]. On the other hand, for Capto S, the apparent h was nearly constant and could not be used to determine D_e since very little of the mAb diffused in the beads.

3.2. Adsorption kinetics

The kinetic mechanisms were expected to be similar for the three mAb fractions because of their similar molecular structures. Thus, the single component adsorption kinetics was studied only for fraction 3 as representative of all three fractions. Uptake curves obtained with different initial protein solution concentrations are shown in Fig. 2a and b for UNOsphere S and Capto S, respectively. Despite the larger binding capacity, larger particle size, and smaller apparent pore size of Capto S, the time needed to attain equilibrium was considerably shorter than for UNOsphere S, indicating faster adsorption kinetics, especially at low protein concentrations. For example at 0.5 mg/ml protein, equilibrium was achieved in about 2000 s for Capto S, while it took more than 6000 s for UNOsphere S. Moreover, the Capto S uptake curves became almost independent of the initial protein concentration above 0.5 mg/ml while significant differences between 1 and 2 mg/ml could be seen for UNOsphere S.

Figs. 3 and 4 show the simultaneous adsorption kinetics for mixtures of mAb fractions 2 and 3 in different ratios at an initial total combined protein concentration of 2 mg/ml for UNOsphere S and Capto S, respectively. As for the single component case, the two-component uptake kinetics were also very different for the two matrices. As seen in Fig. 3, the UNOsphere S uptake curve for fraction 2, which is more deamidated and more weakly bound, always presented an overshoot in the amount bound before gradually returning to equilibrium. This behavior indicates a continuous displacement of fraction 2 by the more strongly bound fraction 3. Conversely, as seen in Fig. 4, the Capto S uptake curves were qualitatively similar for both components in that the final equilibrium value was reached gradually with no apparent overshoot of weakly bound species. The preferential binding for fraction 3 over fraction 2 was nonetheless still evident from the higher equilibrium uptake of the less deamidated fraction 3, consistent with the equilibrium measurements described in Part I of this work [1].

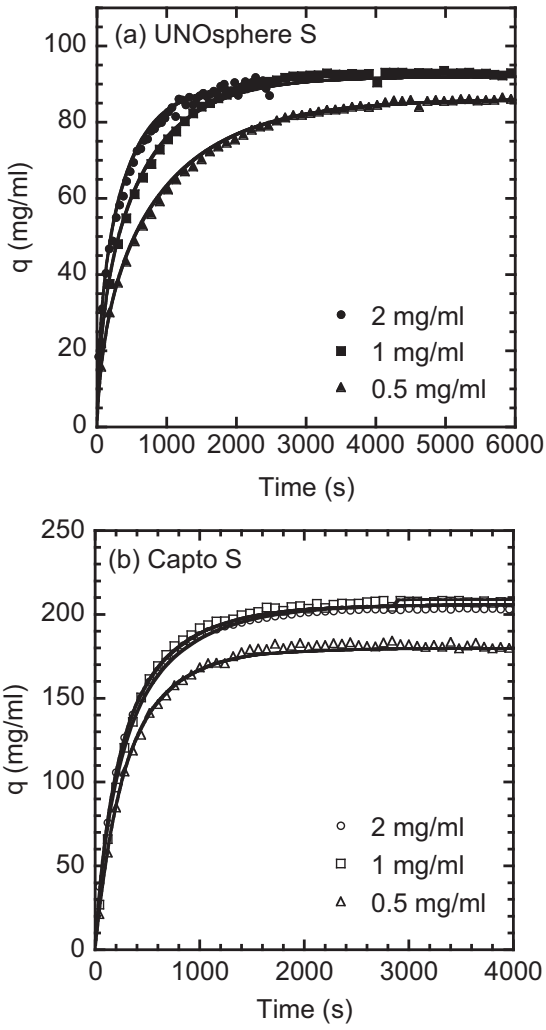

Fig. 2. Batch uptake curves for mAb fraction 3 on UNOsphere S (a) and Capto S (b) at different initial protein concentrations and 0 mM NaCl. Curves are model predictions based on the pore diffusion model with individual D_e-value fitted at each initial protein concentration.

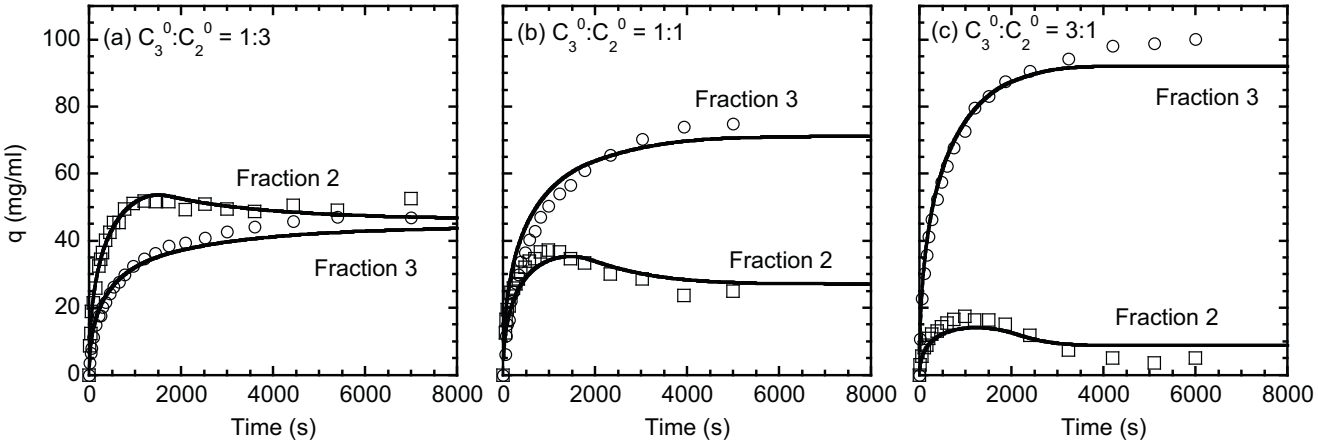

Fig. 3. Simultaneous adsorption of mixtures of mAb fractions 2 and 3 in different initial ratios on UNOsphere S at 0 M NaCl. The total combined initial protein concentration was 2 mg/ml. Lines are predictions based on the pore diffusion model (Eqs. (4) and (5)).

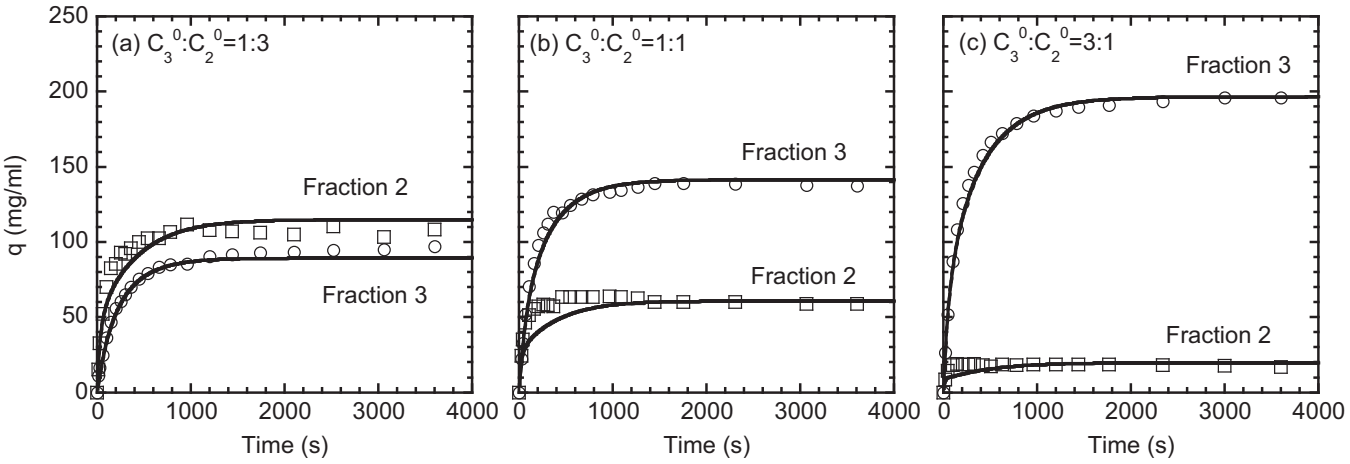

Fig. 4. Simultaneous adsorption of mixtures of mAb fractions 2 and 3 in different initial ratios on Capto S at 0 M NaCl. The total initial protein concentration was 2 mg/ml. Lines are predictions based on the adsorbed phase diffusion model (Eqs. (7) and (8)).

Fig. 5 shows the simultaneous adsorption experiments for mixtures of all three mAb fractions. As seen in Fig. 5a, UNOsphere S showed an overshoot for both fractions 1 and 2. The overshoot was more pronounced for fraction 1, which is the most deamidated and binds most weakly. As seen in Fig. 5b, Capto S again showed no significant overshoot of the amount bound for either fraction 1 or 2 indicating that, in this case, the different species co-diffused in the beads following similar trends as a function of time but attaining different final equilibrium capacities. For both matrices, the time scales of the two- and three-component uptake experiments were similar to the corresponding single component cases, with the Capto S kinetics being considerably faster than for UNOsphere S.

Fig. 6 shows the sequential adsorption results for particles that were first exposed to 1 mg/ml of mAb fraction 2 and then, after attaining equilibrium, to fraction 3. The latter was added as a bolus to give an initial concentration also of 1 mg/ml. This process mimics what is likely to happen in the frontal loading of a mixture of the two components to a column where the weakly bound species is concentrated downstream of the feed front. For both materials, fraction 3 displaced the pre-adsorbed fraction 2. However, this process occurred over very different time scales for the two matrices. As seen in Fig. 6a, for UNOsphere S the displacement kinetics occurred on the same time scale as that of the single-component and simultaneous multicomponent binding processes (~6000 s). Moreover, the fraction 3 uptake curve in the two-component sequential adsorption experiment was very similar to that obtained with a clean resin sample indicating that the presence of pre-adsorbed mAb fraction 2 did not significantly affect transport of the fraction 3 molecules. On the other hand, the Capto S result was quite different. In this case, sequential adsorption on particles that were pre-saturated with mAb fraction 2 occurred over a time scale (≫12,000 s) that was much longer than that observed for the single and two-component simultaneous adsorption experiments. This result suggests that the pre-adsorbed fraction 2 molecules strongly hindered the adsorption kinetics of fraction 3.

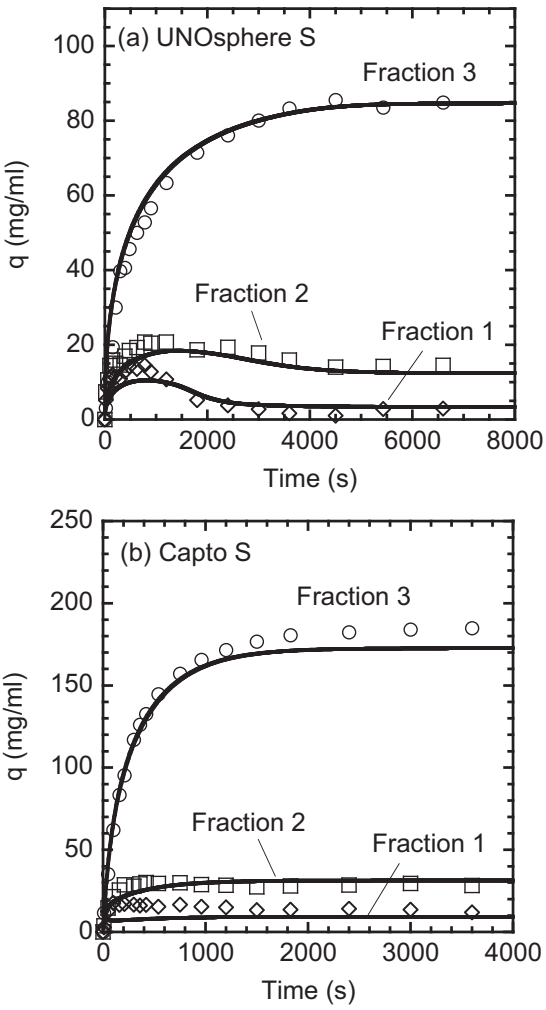

Fig. 5. Simultaneous adsorption of three mAb fractions on UNOsphere S (a) and Capto S (b) with initial protein concentrations $C_1^0 = 0.5$, $C_2^0 = 0.5$, and $C_3^0 = 1$ mg/ml for fractions 1, 2, and 3, respectively, at 0 M NaCl. Lines are predictions based on the pore diffusion model (Eqs. (4) and (5)) for UNOsphere S and on the adsorbed phase diffusion model (Eqs. (7) and (8)) for Capto S.

3.3. Kinetics modeling

Two different models were used to quantitatively describe the adsorption kinetics. The first assumes that pore diffusion is controlling and is given by the following equations and boundary

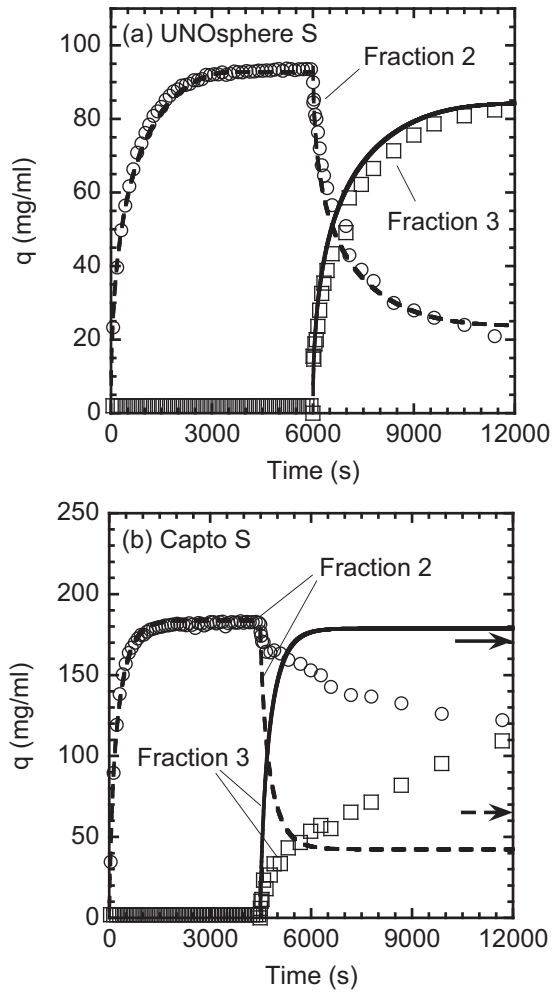

Fig. 6. Sequential adsorption of 1 mg/ml mAb fraction 2 followed by 1 mg/ml fraction 3 on UNOsphere S (a) and Capto S (b) at 0 M NaCl. Lines are predictions based on the pore diffusion model (Eqs. (4) and (5)) for UNOsphere S and on the adsorbed phase diffusion model (Eqs. (7) and (8)) for Capto S. Dashed line is for fraction 2 and solid line is for fraction 3. Arrows in b show the 48 h results.

conditions [11,29]:

$$\frac{\partial q_i}{\partial t} = \frac{D_{e,i}}{r^2}\frac{\partial}{\partial r}\left(r^2\frac{\partial c_i}{\partial r}\right) \tag{4}$$

$$\left.\frac{\partial c_i}{\partial r}\right|_{r=0} = 0 \tag{4a}$$

$$D_{e,i}\left.\frac{\partial c_i}{\partial r}\right|_{r=r_p} = k_{f,i}(C_i - c_i|_{r=r_p}) \tag{4b}$$

$$V\frac{dC_i}{dt} = -\frac{3V_M}{r_p}D_{e,i}\left.\frac{\partial c_i}{\partial r}\right|_{r=r_p} \tag{5}$$

$$C_i|_{t=0} = C_i^0 \tag{5a}$$

where C_i and c_i are the protein concentrations in the bulk liquid and particle pores, respectively, q_i is the adsorbed protein concentration, and $k_{f,i}$ is the external film mass transfer coefficient. q_i and c_i were assumed to be in equilibrium with their relationship expressed by the steric mass action (SMA) model [42] as discussed in Part I of this work:

$$c_i = \frac{q_i C_l^{z_i}}{K_{e,i}[q_0 - \sum(z_i+\sigma_i)q_i]^{z_i}} \tag{6}$$

where q_0 is the resin's ionic capacity, C_l is Na^+ concentration, z_i and σ_i are the effective binding charge and hindrance parameters, respectively, for each protein form, and $K_{e,i}$ is the corresponding equilibrium binding constant. These parameters were obtained from the single component adsorption isotherms and are given in Part I of this work. The same parameters are used for the multicomponent case with the summation in Eq. (6) extended to all mAb components, but not to the Na^+ counterion, which is considered to be in equivalent excess.

The second model assumes that diffusion in the adsorbed phase is controlling. Neglecting accumulation in the pore volume, this model is given by the following equations and boundary conditions:

$$\frac{\partial q_i}{\partial t} = \frac{D_{s,i}}{r^2}\frac{\partial}{\partial r}\left(r^2\frac{\partial q_i}{\partial r}\right) \tag{7}$$

$$\left.\frac{\partial q_i}{\partial r}\right|_{r=0} = 0 \tag{7a}$$

$$D_{s,i}\left.\frac{\partial q_i}{\partial r}\right|_{r=r_p} = k_{f,i}(C_i - C_i^s) \tag{7b}$$

$$V\frac{dC_i}{dt} = -\frac{3V_M}{r_p}D_{s,i}\left.\frac{\partial q_i}{\partial r}\right|_{r=r_p} \tag{8}$$

$$C_i|_{t=0} = C_i^0 \tag{8a}$$

where C_i^s is the fluid phase concentration at the particle surface and is related to $q_i|_{r=r_p}$ through Eq. (6). Both models were solved numerically by finite differences and the solutions compared with the single component uptake curves to determine either D_e or D_s by data fitting. For this purpose, uptake curves were calculated in small increments for a range of values of D_e and D_s. The best-fit values were chosen as those that minimized the sum of residual squares between predicted and experimental values. Average relative deviations between calculated and experimental curves were less than ±3% for either model. Estimated errors of the regressed parameters were based on the D_e- and D_s-values that resulted a ±10% variation of the sum of residual squares. In both cases, the mass transfer coefficient k_f was estimated to be 0.0015 cm/s for all mAb forms based on the results in Ref. [28], although this parameter had practically no effect on the results.

The fitted diffusivity values (D_e and D_s for the pore and adsorbed phase diffusion model, respectively) are shown in Table 1. As previously noted for other systems (e.g. [12–14]), either model could provide a good fit of the batch uptake curves. However, as seen from Table 1, the trends of the fitted parameters as a function of initial protein concentration were different for the two stationary phases both qualitatively and quantitatively. For UNOsphere S, D_e was low and increased only by a relatively small amount as the initial protein concentration was increased. The value $(6.6 \pm 0.3) \times 10^{-8}$ cm^2/s obtained at 2 mg/ml is very close to the value of $(6.8 \pm 0.3) \times 10^{-8}$ cm^2/s determined chromatographically for non-binding conditions. On the other hand, the D_s-value required to fit the UNOsphere S data increased as the protein concentration increased. The opposite behavior was seen for Capto S. In this case, D_e increased as the protein concentration decreased, while D_s remained relatively constant. Beside the trends with protein concentration, the most striking difference was the relatively low values of D_e for UNOsphere S and the relatively high values of D_e for Capto S, in direct contradiction to their respective apparent pore sizes.

The different behavior observed for the two different adsorbents indicates that the underlying transport mechanisms are different. While neither model provided an exact description with constant parameter values, it is apparent that pore diffusion was more consistent (both qualitatively and quantitatively) with the UNOsphere

Table 1
Summary of diffusivity values determined from the single-component uptake curves. D_e are based on Eqs. (4) and (5) while D_s-values are based on Eqs. (7) and (8). Estimated errors of the regressed parameters are based on the D_e- and D_s-values that resulted a ±10% variation of the sum of residual squares.

C_0 (mg/ml)	UNOsphere S			Capto S		
	q^* (mg/ml)	D_e (10^{-7} cm^2/s)	D_s (10^{-9} cm^2/s)	q^* (mg/ml)	D_e (10^{-7} cm^2/s)	D_s (10^{-9} cm^2/s)
0.5	87	1.25 ± 0.03	0.98 ± 0.03	180	10.0 ± 1.0	4.0 ± 0.4
1.0	90	0.83 ± 0.03	1.40 ± 0.10	205	6.0 ± 0.5	4.5 ± 0.4
2.0	93	0.66 ± 0.03	2.0 ± 0.10	205	3.7 ± 0.4	4.1 ± 0.1

S behavior while adsorbed phase diffusion seemed to be a better predictor of the Capto S behavior. An improved prediction may have been obtained for UNOsphere S assuming a small contribution of a parallel surface diffusion flux. The latter, however, appeared to become insignificant at higher protein concentrations since even at just 2 mg/ml the effective pore diffusivity approached the limiting value obtained for non-binding conditions where surface diffusion is impossible.

Prediction of the multicomponent kinetic behavior based on the parameters and models determined from the single-component uptake curves is of interest since, on one hand, multicomponent modeling is useful for design, while, on the other, comparison with the experimental results can shed further light on the underlying transport mechanisms. Calculations were carried out for both the pore diffusion model (i.e. Eqs. (4) and (5)) and for the adsorbed phase diffusion model (i.e. Eqs. (7) and (8)) for each material. However, the surface diffusion model failed to predict the overshoots seen experimentally for UNOsphere S, while the pore diffusion model predicted overshoots not seen experimentally for Capto S. Thus, for simplicity, we only show the predictions of the pore diffusion model for UNOsphere S and those for the adsorbed phase diffusion model for Capto S. The calculations were done using the values of D_e and D_s, for UNOsphere S and Capto S, respectively, obtained with 1 mg/ml initial protein concentration. The results are shown in Figs. 3–6. For simultaneous adsorption with either two or three components (Figs. 3–5, respectively), predictions based on the pore and adsorbed phase diffusion models were in agreement with the experimentally observed trends for UNOsphere S and Capto S, respectively. Average relative deviations between experimental and predicted q-values were ±13% and ±9.3% for UNOsphere S and Capto S, respectively, for the two component cases and ±18% and ±20% for UNOsphere S and Capto S, respectively, for the three component cases. However, as seen in Fig. 6, while the pore diffusion model also predicted the sequential adsorption kinetics for UNOsphere S with accuracy similar to that of the simultaneous adsorption cases, the adsorbed phase diffusion model completely failed to predict the experimentally observed sequential adsorption behavior for Capto S. For the latter, the kinetics of adsorption upon the addition of the second mAb variant was much slower than those predicted by the model and even much slower than those observed and predicted for UNOsphere S.

Finally, an attempt was made to describe the Capto S adsorption kinetics with the model of Lewus and Carta [38] assuming that the mass transfer flux is proportional to the chemical potential gradient. For our system, this model could describe the single and multicomponent simultaneous adsorption kinetics with accuracy similar to that of Eqs. (7) and (8). However, the prediction of sequential adsorption based on this model, while improved somewhat relative to the constant D_s case, also failed to describe quantitatively the very slow kinetics of the sequential adsorption process shown in Fig. 6b.

4. Discussion and conclusions

The experimental results and our analyses based on pore and adsorbed phase diffusion models suggest that the kinetic mechanisms are very different in UNOsphere S and Capto S. Because of the large pore size relative to the molecular size of the mAb, the UNOsphere S adsorption kinetics is dominated by pore diffusion. Not only was the D_e determined from the batch uptake curves a fraction of the free solution diffusivity, but, at relatively higher protein concentrations, D_e became nearly coincident with the value determined for non-binding conditions indicating that protein–surface interactions play only a small role on protein transport in this material. For these conditions, predictions of the multicomponent adsorption kinetics compared well with the experimental behavior for both simultaneous and sequential adsorption confirming that the pore diffusion is still dominant and that the process of displacing one adsorbed variant by another occurs on time scales that are much shorter than that of the overall kinetic process. For this mechanism, similar results with a temporary overshoot are expected to occur whenever a weak binding protein is competitively displaced by a more strongly bound species, regardless of their relative molecular size.

Capto S, on the other hand, behaved differently. For non-binding conditions the dextran-grafted architecture of this material largely excluded the mAb molecules. On the other hand, for conditions where interaction between the positively charged mAb molecules and the negatively charged grafts became highly favorable, these same dextran grafts enhanced both single-component and simultaneous two- and three-component adsorption kinetics, seemingly as a result of a larger driving force. Similar behavior was observed previously for other commercial [43,44] and experimental [23,26,28] dextran-grafted matrices. However, the same enhancement was not seen when a pre-adsorbed, less strongly bound variant was displaced by a more strongly bound one. In this case, the kinetics switched from being very fast to being extremely slow in a manner that could not be predicted by the same model. The reasons for this behavior are not known. One possibility is that the sequential adsorption kinetics in Capto S is associated with a large kinetic resistance when the pre-adsorbed variants are exchanged for more strongly bound ones. However, since these variants are similar and binding is non-specific, such a resistance seems unlikely. Another possibility is that transport in Capto S is controlled by electrostatic coupling of diffusion fluxes between the adsorbing protein molecules and the much faster diffusing Na^+ counterions, as previously hypothesized by Stone et al. [23] for other experimental dextran-grafted matrices. Accordingly, if the highly charged protein molecules retain diffusional mobility in the adsorbed state, protein transport can theoretically be enhanced by the counterdiffusing Na^+ ions as a result of the electrical potential gradient generated by the vast differences in ionic mobility [45]. This would occur whether one component or multiple species are simultaneously adsorbed resulting in a rapid kinetics in both cases. On the other hand, it is clear that such a mechanism could not contribute to the sequential adsorption case where one slowly diffusing component is displaced by another slowly diffusing one having a very similar charge. No rate enhancement associated with electrokinetic effects could take place in this case since exchange for rapidly diffusing Na^+ ions does not occur. The result is then a very slow kinetic process controlled by the highly hindered diffusion similar to that seen experimentally for non-binding conditions. This putative mecha-

nism, however, requires diffusional mobility in the adsorbed phase where the protein concentration can reach sufficiently high values for diffusional flux coupling to be significant. As such, it is not likely to be significant at high salt, where the adsorbed protein concentration is very low, or in the liquid phase. Conceptually, this mechanism appears to be consistent with the experimental results. A quantitative analysis is however beyond the scope of this work since the relationships describing coupled ionic transport are most likely complicated by the currently unknown intrusion of co-ions in the resin matrix [45]. A third possibility is that protein transport in Capto S is associated with the dynamic behavior of the grafted dextran polymers. Cussler et al. [46], for example, have discussed a potential mechanism for porous membranes containing tethered carriers where solute transport is facilitated by local fluctuations, which pass molecules from one carrier to the next in a manner akin to a "bucket brigade". Unfortunately, however, to our knowledge, no fundamentally based model is currently available to describe this process. As a result we cannot currently test this hypothesis.

From a practical viewpoint, this work, combined with the conclusions in [1], offers valuable clues about the relative advantages of macroporous and dextran grafted matrices and shed light on what models can be used to predict their respective behavior on actual process separations. However, while the UNOsphere S behavior is likely to be similar to that observed in this work for other competitively bound proteins, predicting the behavior of Capto S for other systems could be challenging since the interactions of the charged dextran grafts with the diffusing proteins could be highly dependent on the specific molecular properties of each system.

Nomenclature

c	concentration in particle pores (mg/ml or mM)
C	fluid phase concentration (mg/ml or mM)
C_I	Na^+ concentration (mM)
d_p	particle diameter (cm)
D_e	effective pore diffusivity (cm^2/s)
D_s	adsorbed phase diffusivity (cm^2/s)
D_0	free solution diffusivity (cm^2/s)
h	reduced HETP (=HETP/d_p)
k'	chromatographic retention factor
k_f	external film mass transfer coefficient (cm/s)
K_e	equilibrium constant for protein–counterion exchange in SMA model
q	adsorbed concentration (mg/ml or mM)
q^*	adsorbed concentration in equilibrium with external solution (mg/ml or mM)
q_0	charge density of stationary phase (mM)
r	particle radial coordinate (cm)
r_p	particle radius (cm)
t	time (s)
ν	mobile phase interstitial velocity (cm/s)
ν'	reduced velocity ($= \nu d_p/D_0$)
V	solution volume (ml)
V_M	volume of particles (ml)
z	protein effective binding charge
ε	extraparticle void fraction
ε_{pM}	intraparticle macroporosity
ψ_p	diffusional hindrance factor
σ	hindrance parameter in SMA model
τ_p	tortuosity factor

Subscript

i	component number

Superscripts

0	initial value
S	value at the particle surface

Acknowledgements

This research was supported by MedImmune and NSF Grant Nos. CTS-0729857 and CBET-1032727.

References

[1] Y. Tao, G. Carta, G. Ferreira, D. Robbins, J. Chromatogr. A 1218 (2011) 1519–1529.
[2] R.J. Harris, B. Kabakoff, F.D. Macchi, F.J. Shen, M. Kwong, J.D. Andya, S.J. Shire, N. Bjork, K. Totpal, A.B. Chen, J. Chromatogr. B 752 (2001) 233.
[3] H. Liu, G. Gaza-Bulseco, C. Chumsae, Rapid Commun. Mass Spectrom. 22 (2008) 4081.
[4] A.C.A. Roque, C.R. Lowe, M.A. Taipa, Biotechnol. Progr. 20 (2004) 639.
[5] N. Tugcu, D.J. Roush, K.E. Goklen, Biotechnol. Bioeng. 99 (2008) 599.
[6] M. Weitzhandler, D. Farnan, J. Horvath, J.S. Rohrer, R.W. Slingsby, N. Avdalovic, C. Pohl, J. Chromatogr. A 828 (1998) 365.
[7] M. Perkins, R. Theiler, S. Lunte, M. Jeschke, Pharm. Res. 17 (2000) 1110.
[8] M. Weitzhandler, D. Farnan, J.S. Rohrer, N. Avdalovic, Proteomics 1 (2001) 197.
[9] L. Melter, G. Strohlein, A. Butte, M. Morbidelli, J. Chromatogr. A 1154 (2007) 121.
[10] M.E. Ladisch, Bioseparations Engineering – Principles, Practice and Economics, Wiley Interscience, New York, USA, 2001.
[11] G. Carta, A. Jungbauer, Protein chromatography–Process development and Scale-up, Wiley-VCH, Weinheim, Germany, 2010.
[12] G. Carta, A.R. Ubiera, T.M. Pabst, Chem. Eng. Technol. 28 (2005) 1252.
[13] A.M. Lenhoff, Langmuir 24 (2008) 5991.
[14] L.E. Weaver, G. Carta, Biotechnol. Progr. 12 (1996) 342.
[15] C. Chang, A.M. Lenhoff, J. Chromatogr. A 827 (1998) 281.
[16] R.K. Lewus, G. Carta, J. Chromatogr. A 865 (1999) 155.
[17] S.R. Dziennik, E.B. Belcher, G.A. Barker, M.J. de Bergalis, S.E. Fernandez, A.M. Lenhoff, Proc. Natl. Acad. Sci. U.S.A. 100 (2003) 420.
[18] X.P. Zhou, W. Li, Q.H. Shi, Y. Sun, J. Chromatogr. A 1103 (2006) 110.
[19] E.B. Schirmer, G. Carta, AIChE J. 53 (2007) 1472.
[20] M.C. Stone, G. Carta, J. Chromatogr. A 1160 (2007) 206.
[21] A.K. Hunter, G. Carta, J. Chromatogr. A 971 (2002) 105.
[22] S.R. Dziennik, E.B. Belcher, G.A. Barker, A.M. Lenhoff, Biotechnol. Bioeng. 91 (2005) 139.
[23] M.C. Stone, Y. Tao, G. Carta, J. Chromatogr. A 1216 (2009) 1216.
[24] R.K. Lewus, G. Carta, Ind. Eng. Chem. Res. 40 (2001) 1548.
[25] S. Russell, E.B. Belcher, G. Carta, AIChE J. 49 (2003) 1168.
[26] M.C. Stone, G. Carta, J. Chromatogr. A 1146 (2007) 202.
[27] K. Yang, Y. Sun, Biochem. Eng. J. 37 (2007) 298.
[28] Y. Tao, G. Carta, J. Chromatogr. A 1211 (2008) 70.
[29] M.D. LeVan, G. Carta, in: D.W. Green (Ed.), Perry's Chemical Engineers' Handbook, 8th ed., McGraw-Hill, New York, 2007 (Section 16).
[30] R.J. Phillips, W.M. Deen, J.F. Brady, AIChE J. 35 (1989) 1761.
[31] F.G. Smith, W.M. Deen, J. Coll. Int. Sci. 91 (1983) 571.
[32] H. Yoshida, M. Yoshikawa, T. Kataoka, AIChE J. 40 (1994) 2034.
[33] A.K. Hunter, G. Carta, J. Chromatogr. A 897 (2000) 81.
[34] P.D. Robbins, A dynamic approach to protein purification by adsorption, PhD Thesis, Massachusetts Institute of Technology, Cambridge, MA, USA, 1989.
[35] C. Martin, G. Iberer, A. Ubiera, G. Carta, J. Chromatogr. A 1079 (2005) 105.
[36] T. Linden, A. Ljunglof, M.R. Kula, J. Thommes, Biotechnol. Bioeng. 65 (1999) 622.
[37] S.R. Gallant, J. Chromatogr. A 1028 (2004) 189.
[38] R.K. Lewus, G. Carta, AIChE J. 45 (1999) 512.
[39] S.M. Russell, G. Carta, AIChE J. 51 (2005) 2469.
[40] N. Forrer, A. Butte, M. Morbidelli, J. Chromatogr. A 1214 (2008) 71.
[41] E.L. Cussler, Diffusion – Mass Transfer in Fluid Systems, 2nd ed., Cambridge University Press, Cambridge, UK, 1997.
[42] C.A. Brooks, S.M. Cramer, AIChE J. 38 (1992) 1969.
[43] J. Thommes, Biotechnol. Bioeng. 61 (1999) 358.
[44] A. Ubiera, G. Carta, Biotechnol. J. 1 (2006) 665.
[45] F. Helfferich, Ion Exchange, McGraw-Hill, New York, USA, 1962.
[46] E.L. Cussler, R. Aris, A. Bhown, J. Membr. Sci. 43 (1989) 149.